# Rectification of energy and motion in active gyroscopic networks

Zhenghan Liao,[1] William Irvine,[2] and Suriyanarayanan Vaikuntanathan[3]

[1] *Department of Chemistry, University of Chicago, Chicago, IL, 60637, USA*
[2] *James Franck Institute, Enrico Fermi Institute and Department of Physics, University of Chicago, Chicago, IL, 60637, USA*
[3] *James Franck Institute and Department of Chemistry, University of Chicago, Chicago, IL, 60637, USA*

## Abstract

[Will be revised in the end] We study a model that combines gyroscopic networks and active matter. From numerical calculations, theory, and simulations, we show that autonomous heat flows are generated at the nonequilibrium steady state. Distinct from conventional heat flows that are driven by temperature difference at the boundaries, this heat flow is an emergent collective behavior. We then focus on understanding three issues: the mechanism of this nonzero heat flow, the connection between the flow in active system and that in the well-studied isolated system, and the relationship between the network geometry and the flow pattern. Understanding the last issue in turn enables us to control the flow pattern by the design of the network geometry.

## I. INTRODUCTION

Uncovering principles that can enable the rectification of stochastic fluctuations has been a long standing problem in non-equilibrium statistical mechanics [1, 2]. The Feynman Ratchet and pawl model, and its associated generalizations, have elucidated how systems can rectify stochastic fluctuations and act as microscopic engines that perform work and exert forces [3]. Indeed such models have provided a framework to understand how biological molecular motors can convert the energy derived from the hydrolysis of energy rich molecules into mechanical work [4–7]. While these advances provide powerful design principles, especially for rectification in single-body systems, we still have very few design principles to engineer rectification in many body systems [1], particularly in the absence of any imposed asymmetries.Uncovering such principles can, for instance, identify methods to manipulate the flow of energy across materials without any imposed temperature biases [8–13]. They can also potentially facilitate the development of design principles for constructing synthetic molecular motor analogues. In this paper, we establish a new and general set of principles for how such rectification can be achieved in parity violating many body interacting systems. In particular, we show how a parity violating meta material [14] can spontaneously rectify energy and motion in the absence of any imposed gradients, when it is allowed to interact with a bath of *active* particles that consume energy to power their motion [15–17].

We construct our design principles using a class of model parity violating meta materials. Our choice of parity violating meta material is inspired by a recent work where a meta material composed of interacting gyroscopes was introduced [14]. These gyroscopic meta materials were shown to support chiral topological edge modes. The topological chiral edge modes can be explained in terms of a violation of time reversal symmetry in the microscopic equations of motion of the interacting gyroscopes [14, 18]. Importantly, the violation of time reversal symmetry is controlled by an interplay between the spin of the gyroscopes and the geometry of the lattice. In the model systems considered in this paper, such parity violating meta materials are allowed to interact with a bath of *active* particles that violate the fluctuation dissipation relation [19].

Our central result shows how a combination of time reversal symmetry violations due to chirality, interactions between the particles of our model system, and time reversal symmetry violations implicit in the single particle fluctuations of the bath that the model system is in contact with, can help rectify stochastic fluctuations. Indeed, naively coupling the topological chiral meta material to a heat bath does not result in any fluxes or symmetry breaking on account of the Bohr-van Leeuwen theorem that forbids any non-equilibrium currents in thermalized magnetic systems. In contrast, we find that our model system can support a directed flux of energy across the network. Unlike conventional energy flows, our energy flow is not supported by a temperature gradient. Moreover, we show that the *parity violating active* network can in fact pump energy through an otherwise isolated elastic object. Finally, we also show that the microscopic mechanisms responsible for this energy flow can also potentially allow the *parity violating active* network to swim in and exert forces on a viscous fluid. We analytically and numerically demonstrate these results for a wide variety of network geometries thus establishing the generality of our results. In particular, we construct an intuitive diagrammatic approach for computing the energy flux (and consequently the swim speed) that shows how our results can readily applied to tailor flows in arbitrarily complex networks. Taken together, our results establish a new set of design principles for rectification of energy, motion and forces in chiral many body systems. Our design principles, unlike many existing prescriptions, exploit inherent asymmetries in the geometry and interactions of the material to achieve rectification.

The remainder of this paper is organized as follows: In Sec. II, we introduce our model active chiral system,

provide a microscopic definition for the energy flux, and present numerical results. In Sec. III-V we analytically identify the ingredients for rectification of energy fluxes and construct a diagrammatic approach that reveals a relationship between energy flux and network geometries. Finally in Sec. VI we show implications of the rectification in the context of low Reynolds number swimming or fluid pumping.

## II. MODEL SYSTEMS AND ENERGY FLUX

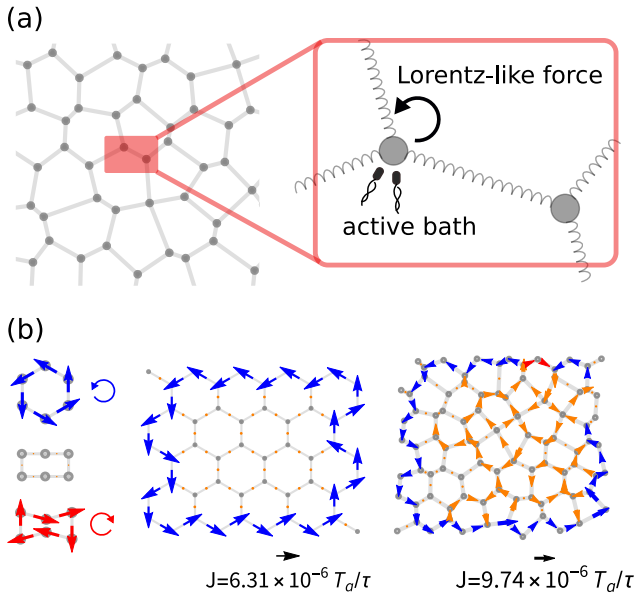


FIG. 1. The model and the energy flux in exemplary networks. (a) Schematic of the model, a spring-mass network with Lorentz-like force and active bath on each particle. (b) Averaged energy flux from numerical calculations for a few typical networks. The flux direction and pattern can be controlled by the network geometry. In these figures, gray lines and dots represent the mechanical equilibrium structure of the network, and arrows represent the direction and magnitude of the averaged energy flux. The arrows are colored blue if it is counter-clockwise (CCW), red if clockwise (CW), and orange otherwise. The flux magnitude is $5.42 \times 10^{-6} T_a/\tau$ for hexagon network and $2.76 \times 10^{-6} T_a/\tau$ for bowtie network. For complex networks, fluxes smaller than 1/10 of the scale bar are not shown for clarity. All parameters are set to 1.

Our model chiral system is a spring-mass network with Lorentz-like force and active bath [19] on each site (FIG. 1a). The equation of motion reads

$$m\dot{\boldsymbol{v}}_i = -k_g \boldsymbol{z}_i + \sum_j \boldsymbol{F}_{ji} + \boldsymbol{v}_i \times \boldsymbol{B} - \gamma \boldsymbol{v}_i + \boldsymbol{\eta}_i, \quad (1)$$

where $z_i \equiv \begin{pmatrix} x_i & y_i \end{pmatrix}^T$ is the displacement of particle $i$ from its mechanical equilibrium position.

The first three terms on the right-hand side describe a spring-mass network with Lorentz force. The first term is the on-site restoring force. The second term is the spring force from the bonded neighbors $j$'s, $F_{ji} = k(e_{ij}^T z_i + e_{ji}^T z_j)(-e_{ij})$. Here the force is linearized by assuming the natural length of springs are much larger than the scale of particles' displacement, and $e_{ij}$ is the unit vector from the equilibrium position of $i$ to that of $j$. The third term $\boldsymbol{v}_i \times \boldsymbol{B}$ is the Lorentz-like force (the electric charge-like factor is absorbed in $\boldsymbol{B}$), and we set $\boldsymbol{B} = -B\hat{\boldsymbol{z}}$. The construction of our model system is motivated by the recently constructed topological gyroscopic metamaterials [14]. Indeed, in the linearized regime, the equations of our model system are equivalent to the equations of motion of the gyroscopic metamaterials [20].

The last two terms describe the active bath, which consists of friction $-\gamma v_i$ and an Ornstein-Uhlenbeck (OU) colored noise $\eta_i$ [19]. The colored noise has finite correlation time $\tau$ and strength $T_a$ ($T_a$ has the unit of energy)

$$\left\langle \eta_i(t) \eta_j^T(t') \right\rangle = I\delta_{i,j} \frac{\gamma T_a}{\tau} e^{-\frac{|t-t'|}{\tau}}, \quad (2)$$

where $I$ is the identity matrix with appropriate dimensions. The time evolution of the OU noise can be described according to the following equation [21],

$$\tau \dot{\eta}_i = -\eta_i + \sqrt{2\gamma T_a}\xi_i, \quad (3)$$

where $\xi_i$ is the standard Gaussian white noise. The friction $-\gamma v_i$ and OU noise $\eta_i$ break fluctuation-dissipation relation, thus driving the system out of equilibrium [19]. The active bath reduces to the familiar Langevin bath in the $\tau \to 0$ limit.

The observable we mainly focus on is the time-averaged energy flux between particles at steady state. For a system with pairwise interactions and on-site potentials, the energy flux $\langle J_{ij} \rangle$ from particle $i$ to $j$ reads

$$\langle J_{ij} \rangle = \left\langle \frac{1}{2}(\mathbf{v}_j \cdot \mathbf{F}_{ij} - \mathbf{v}_i \cdot \mathbf{F}_{ji}) \right\rangle = \langle \mathbf{v}_j \cdot \mathbf{F}_{ij} \rangle . \quad (4)$$

To arrive at this formula, first we define the energy of a particle as the sum of its kinetic energy, on-site potential energy, and one half of the bond energies [22]. Then we write down the energy balance relations using ideas from stochastic energetics [23]. Finally we identify the energy exchanged due to particle-particle interactions as the energy flux $\langle J_{ij} \rangle$. A detailed derivation is provided in the supplemental material. We note that the energy flux can simply be interpreted as the rate at which work is done on particle $j$ by particle $i$. Since this microscopic work is due to particles' stochastic motions, rather than due to an external control, the energy flux can also be interpreted as a heat flux [22, 23]. The averaged energy fluxes are identitically equal to zero for a system at equilibrium.

Starting from the linear equations Eqn. (1), (3), the energy fluxes can be solved numerically using methods introduced in [24, 25] (Supplemental Material). A collection of numerical results are shown in FIG. 1b. We see nonzero energy rectification or energy fluxes can be generated in our chiral active system, and the flux direction

or pattern changes with the network geometry. Using a linear response theory, we now develop analytical expressions for the energy flux. These expressions reveal how a combination of chirality, nonequilibrium activity, and network geometry is responsible for generating energy fluxes.

## III. LINEAR RESPONSE THEORY FOR ENERGY FLUX

We begin by writing the equations of motion, Eqn. (1), in frequency space,

$$\tilde{z}(\omega) = G^{+}(\omega)\tilde{\eta}(\omega), \tag{5}$$

$$G^{+}(\omega) \equiv [K + i\omega(\gamma I + BA) - m\omega^2 I]^{-1}. \tag{6}$$

We represented the displacement of all particles by a column vector $z = \sum_i |i\rangle \otimes z_i$, with $|i\rangle$ denoting the 2D subspace of particle $i$. $\tilde{z}(\omega)$ and $\tilde{\eta}(\omega)$ denote the Fourier transform of $z$ and the OU noise $\eta$, respectively. $G^{+}$ is the response matrix, in which matrix $K$ encodes all onsite and spring forces $F$ according to $F = -Kz$, and $A$ is an antisymmetric matrix $A = \sum_i |i\rangle\langle i| \otimes \begin{pmatrix} 0 & 1 \\ -1 & 0 \end{pmatrix}$. Eqn. (5) describes how the displacement responds to the noise.

Following the procedure in [26], the flux defined in Eqn. (4) can be expressed using $G^{+}$ as a spectral integral (Supplemental Material)

$$\langle J \rangle = \int_{-\infty}^{\infty} \mathrm{d}\omega\, h(\omega) J^{FT}(\omega), \tag{7}$$

$$J^{FT}(\omega) \equiv -\frac{T_a k}{2\pi} \mathrm{Re}\,\mathrm{tr}\, G^{+}(\omega) A^{as}, \tag{8}$$

$$h(\omega) = \frac{1}{1 + \omega^2\tau^2}, \tag{9}$$

where $A^{as}$ is an antisymmetric matrix $A^{as} = -|i\rangle\langle j| \otimes e_{ij}e_{ji}^T + |j\rangle\langle i| \otimes e_{ji}e_{ij}^T$. The response function $G^{+}(\omega)$ has no pole in the lower-half complex plane, but the colored noise introduces one pole at $\omega = -i/\tau$. Using the residue theorem we get a compact expression for the energy flux (Supplemental Material)

$$\frac{\langle J \rangle}{T_a/\tau} = -\frac{k}{2}\,\mathrm{tr}\, G^{+}(-\frac{i}{\tau}) A^{as}. \tag{10}$$

Eqn. (7) and (10) will serve as our starting point to understand the energy flux. While they contain all the information required to compute energy fluxes, they have limited utility as design principles. Indeed, as written down, they require that the flux be recomputed de novo for each new network geometry and non-equilibrium bath activity. In the next sections, we show that it is possible to expand Eqn. (7) and (10) in forms that reveals desgin principles for controlling energy fluxes.

Before moving on, we note that the energy fluxes satisfy Kirchoff's law, $\sum_i \langle J_{ij} \rangle = 0$, i.e. on average there is no energy exchange between particles and the active bath. To derive the Kirchoff's law, we calculate the average heat exchange between particle $i$ and the active bath $\langle \boldsymbol{v}_i \cdot \boldsymbol{\eta}_i - \gamma \boldsymbol{v}_i \cdot \boldsymbol{v}_i \rangle$, and following procedures in [26], this heat exchange can be shown to be zero. The Kirchoff's law puts a strong constraint on possible energy flux patterns among particles, and some corollaries immediately follow, such as networks with no cycles cannot have nonzero flux, and fluxes of all bonds in a polygon network (as in FIG. 1b) are equal.

## IV. INGREDIENTS FOR ENERGY RECTIFICATION AND THEIR ROLES

Compared with an ordinary thermal spring-mass network, which supports no energy fluxes in its equilibrium steady state, our model contains two extra components, the Lorentz force and the correlation in the noise. We first show that these two components provide two necessary ingredients required to ensure energy rectification in our model.

As a prerequisite, we note that the functions $J^{FT}(\omega), h(\omega)$ in Eqn. (7) can be interpreted as follows. The function $J^{FT}(\omega)$ is proportional to the the energy flux at Fourier frequency $\omega$ in an isolated damped variant of our network. The function $h(\omega)$ is proportional to the the noise spectrum, $\langle \tilde{\eta}(\omega)\tilde{\eta}^*(\omega) \rangle = 2\gamma T_a h(\omega)/t$.

### A. Lorentz force and non-equilibrium activity are necessary for the generation of an energy flux

To generate a nonzero flux, or equivalently make the integral nonzero, we need two requirements (FIG. 2a). Firstly, $J^{FT}(\omega)$ should not be zero everywhere (FIG. 2b). If $B = 0$, the response $G^{+}$ is symmetric or reciprocal, and since $A^{as}$ is antisymmetric, the trace $\mathrm{tr}\, G^{+}(\omega)A^{as} = 0$ at all values of $\omega$. Nonzero $B$ breaks the reciprocity of $G^{+}$, thus can generate a nonzero $J^{FT}(\omega)$, or generate chiral Fourier modes.

Nonzero $J^{FT}(\omega)$ alone does not ensure a nonzero averaged energy flux, we further require that $h(\omega)$ should not be constant. If $h(\omega)$ is constant, it corresponds to a white noise, and the system would be in equilibrium according to the Bohr-van Leeuwen theorem [27]. The $h(\omega)$ for the fluctuation dissipation violating OU noise, $h(\omega) = 1/(1 + \omega^2\tau^2)$, provides more weightage to fluxes at smaller values of $\omega$. The resulting average flux can hence potentially be nonzero. We note that other forms of colored noise could have also served the same purpose.

In summary, we see that $B$-field, and a colored noise are two necessary ingredients to generate flux in our model chiral systems. The role of the $B$-field is to break the reciprocity of response and generate Fourier modes such that $J^{FT}(\omega) \neq 0$. The role of the colored noise is to excite these modes in a weighted manner.

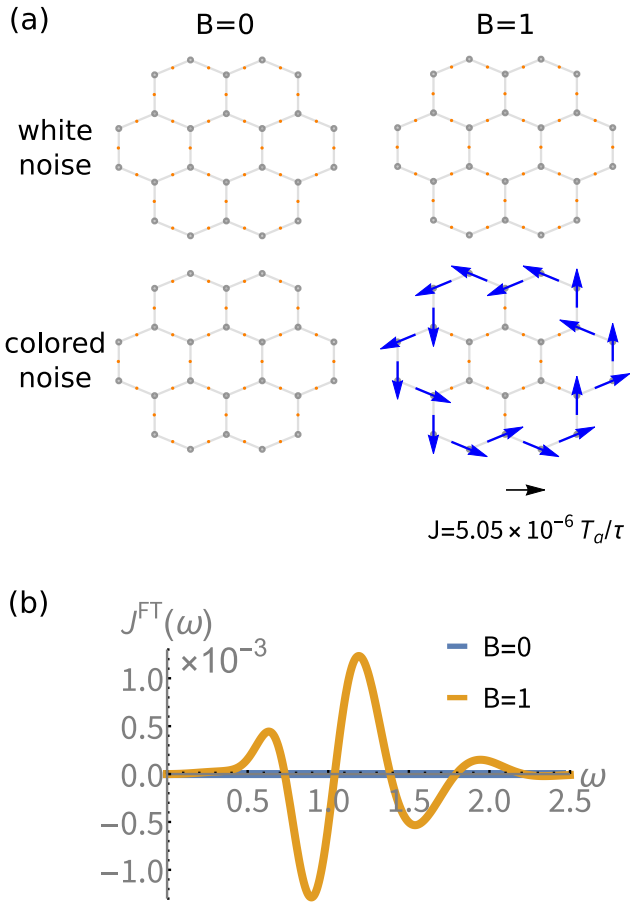


FIG. 2. Necessary ingredients for generating nonzero energy fluxes. (a) Both Lorentz-like force and colored noise are needed to generate nonzero fluxes. (b) Mechanistically, the role of Lorentz-like force is to provide chiral Fourier modes ($J^{FT}(\omega) \neq 0$). If $B = 0$, $J^{FT}(\omega)$ is zero everywhere.

### B. Energy flux can be tuned as a function of lattice geometry

Apart from the these two ingredients, the geometry of the network also plays an important role. Indeed in the small $\gamma$ regime, the existence of chiral modes with $J^{FT}(\omega) \neq 0$ can be heuristically explained by exploiting the connection between the slightly damped isolated variants of our system and the undamped isolated gyroscopic metamaterials [14, 18]. Specifically, the slightly damped variant would resonate near the eigen-frequencies of the undamped metamaterials, and exhibit Fourier modes that are close to the eigenmodes of the undamped system. Consequently, we infer that $J^{FT}(\omega) \neq 0$ as long as the corresponding eigenmodes in the undamped variant are chiral. As discussed in [14], the geometry of the network plays a crucial role in generating the chiral eigenmodes. At larger $\gamma$'s, the Fourier modes of our damped isolated variant are no longer close to the chiral eigenmodes of gyroscopic metamaterials, but a connection between eigenmodes and energy fluxes can still be built (Supplemental Material). In the next section, we further elaborate the role of geometry. Specifically, the central results of the next section provide compact expressions that elucidate the role played by geometry, Lorentz forces and non-equilibrium activity.

## V. RELATIONSHIP BETWEEN FLUX AND NETWORK GEOMETRY

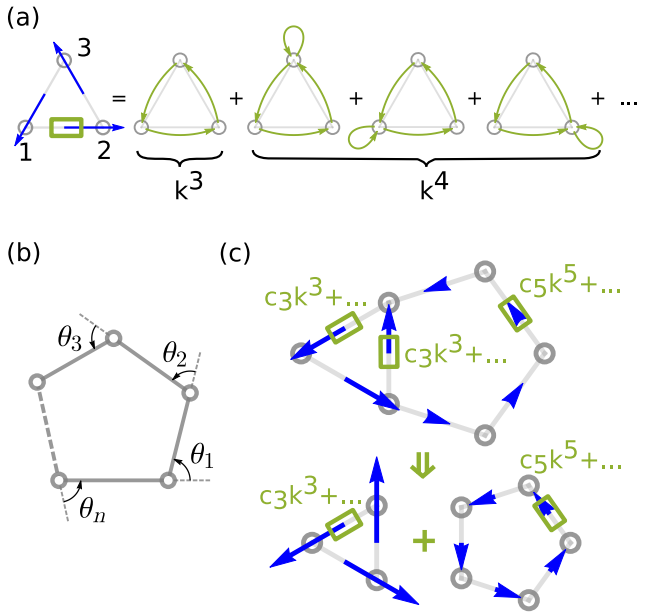


FIG. 3. Illustrations of our diagrammatic technique. (a) Flux from 1 to 2 can be calculated by summing over paths. Each path is a pictorial representation of one term in the small-$k$ expansion, and is depicted using green arrows. The magnitude of path with length $n$ is on the order of $k^n$. (b) Schematic of a polygon path and its outer angles $\theta_1, \theta_2, \ldots, \theta_n$. The flux of this path is simply Eqn. (13). (c) For flux in complex networks, the leading order term is determined by the shortest cycles. Flux in the triangle part has order $k^3$, and the prefactor $c_3$ is the same as that in a standalone triangle network. Likewise for the pentagon part. As a result, the flux in a complex network can be viewed as a combination of fluxes in its constituent cycles.

In this section we develop a diagrammatic technique, which provides a simple intuitive method to compute energy fluxes and reveals a relationship between flux and network geometry. The diagrammatic technique is constructed by expanding the expressions for the energy flux Eqn. (10) in small-$k$ regime and shows how the energy flux across a bond can be expressed as a sum over paths traversed along the network (Eqn. (11)). Our perturbation theory assigns a geometry dependent prefactor for each path, thus elucidating the role played by network geometry in ensuring rectified energy fluxes (Eqn. (13)). Together, the central results of this section, Eqn. 11,

Eqn. 13 provide compact expressions that elucidate how geometry, $B$-field, and correlation time $\tau$ of the colored noise can combine to generate energy flows in networks with arbitrarily complex geometry and topologies.

### A. Path summation and its rules

Starting from the flux formula Eqn. (10), one can expand the flux to different orders in the spring constant $k$. Then for each order, one can further expand to different paths. As a result, the total flux can be written as a sum over the flux of paths (FIG. 3a), (Supplemental Material)

$$\frac{\langle J\rangle}{T_a/\tau} = \sum_l J_l^{\text{path}} = \sum_l \frac{1}{2}(S_l - S_{-l}). \tag{11}$$

The path rules are as follows. For the flux from $i$ to $j$, valid paths are $l = i \to j \to l_3 \to l_4 \to \cdots \to l_n \to i$, where $l_a$ and $l_b$ either has to be bonded or $l_a = l_b$. Paths that contain equal numbers of $i \to j$ and $j \to i$ do not contribute (e.g. path $i \to j \to i$), because either the path itself vanishes or it cancels with another path. As a result, paths appear as cycles. The term $S_l$ is defined as $S_l \equiv (\frac{k}{k_0})^n \operatorname{tr} R_\alpha(-K_s)_{il_n} \cdots R_\alpha(-K_s)_{l_3 j} R_\alpha(-K_s)_{ji}$. In this definition, $k_0 \equiv \sqrt{(k_g + \gamma/\tau + m/\tau^2)^2 + (B/\tau)^2}$ sets a characteristic scale for spring constant $k$. $R_\alpha$ is a CCW rotation by angle $\alpha$, defined as

$$\alpha = \arcsin \frac{B/\tau}{k_0}. \tag{12}$$

The factor $\alpha$ condenses all the geometry independent parameters into one angle. $(K_s)_{l_b l_a} \equiv \langle l_b | (K - k_g I) | l_a \rangle / k$ is a non-dimensionalized spring force on $l_b$ due to the displacement of $l_a$. $-l$ means $l$ in the reversed order. The interval of convergence depends on the geometry of the whole network as well as the parameter $\alpha$. The typical value of the upper bound of $k/k0$ ranges between 0.3 and 0.6.

The paths can be represented using diagrams, from which the flux $J_l^{\text{path}}$ can be calculated easily. For instance, the first diagram in FIG. 3a represents the path $1 \to 2 \to 3 \to 1$. To calculate $S_l$, one writes $(-K_s)_{l_b l_a}$ for each arrow $l_a \to l_b$, $R_\alpha$ for each node $l_a$, then multiply these matrices in the reversed order, and calculate the trace, e.g. $S_{1\to2\to3\to1} = (k/k_0)^3 \operatorname{tr} R_\alpha(-K_s)_{13} R_\alpha(-K_s)_{32} R_\alpha(-K_s)_{21}$. To get $S_{-l}$, one takes the result of $S_l$ and replace $\alpha$ by $-\alpha$. Finally, $J_l^{\text{path}}$ can be calculated from the difference between $S_l$ and $S_{-l}$.

### B. Contributions to energy flux from polygonal paths

Path with length $n$ is on the order $(k/k_0)^n$. In the small $k$ regime, the main contribution to the flux comes from the lowest-order paths. The usual lowest-order paths are polygonal cycles with no loops (loops are self-connecting edges, $l_a \to l_a$). In this case, the formula for $J_l^{\text{path}}$ Eqn. (11) reduces to a simple form (Supplemental Material)

$$J_{\text{polygon}}^{\text{path}} = \frac{1}{2}(\frac{k}{k_0})^n (\prod_i \cos(\theta_i - \alpha) - \prod_i \cos(\theta_i + \alpha)), \tag{13}$$

where $\alpha$ is defined in Eqn. (12), $n$ is the number of nodes and $\theta_i$'s are outer angles (FIG. 3b). Eqn. 13 illustrates how geometry of the network, as characterized by the angles $\theta_i$, together with the condensed parameter $\alpha$ that encodes the nonreciprocity due to the $B$ field and the violation of fluctuation dissipation due to the colored noise, combine to generate energy fluxes.

For polygon networks, Eqn. (13) gives a direct relationship between the lowest-order flux and the network geometry. As an example, flux in an arbitrary triangle is $J \propto k^3 \sin\theta_1 \sin\theta_2 \sin\theta_3 + \mathcal{O}(k^4)$, whose $k^3$ term is always positive or CCW. For complex networks, Eqn. (13) implys that its lowest-order flux can be viewed as a result of combining the flux of its constituent polygons, as illustrated in FIG. 3c. This is because the flux of a polygonal path Eqn. (13) is not affected by any side chains on the nodes, and $J_{\text{polygon}}^{\text{path}}$ for a polygon in a complex network is the same as $J_{\text{polygon}}^{\text{path}}$ for the polygon when standalone.

Starting from the diagrammatic expansion, the presence of localized energy fluxes in some networks (FIG. 1b) can be readily understood. Consider for instance the paths contributing to flux along an edge in a honeycomb-like network. Away from the boundary, the lower order path contributions to the energy flux cancel each other, and higher order path contributions become dominant. The size of the leading order path that contributes to the energy flux along a bond increases as a function of the distance of the bond from boundary. Such a scaling results in an exponential localization of the energy flux at the boundary of the network.

More generally, using these decompositions, it is easy to program energy flux patterns in networks of arbitrary complexity. Our diagrammatic expansion hence allows us to go beyond the need for de novo calculations suggested by our previous expressions.

## VI. NON-RECIPROCAL MOTIONS RESPONSIBLE OF ENERGY FLUXES CAN BE USED TO GENERATE FORCES

The rectification of energy has been our main focus so far. In this section, we show that it possible to exploit the energy flux to rectify motions when our model systems are allowed to interact with a viscous fluid. We begin by demonstrating that a *passive* segment –this segment does not experience Lorentz force or active bath so that it is completely ordinary –when coupled to our chiral active network, supports an energy flux. Next we used

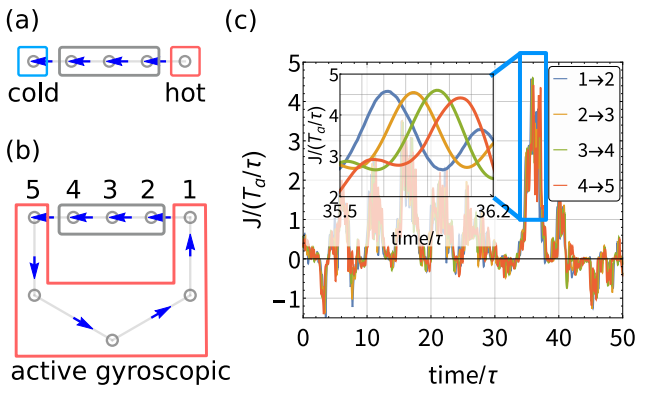


FIG. 4. Driving energy through an elastic chain (a) Conventional heat conduction in a chain with temperature differences at two ends. The temperature difference drives a heat flow through a passive material (boxed in gray). (b) Similar to (a), the active gyroscopic network can also drive energy flows through a passive segment. In the simulation setup, the separation between active particles (boxed in red) is large compared with the length-scale of their displacements, and their parameters are: $m, k_g, \gamma = 0.1, k = 10$, others are 1. Passive particles (boxed in gray) are constrained to 1D, and their $\gamma, T_a, k_g$ are set to 0. (c) Instantaneous energy flux $\langle J \rangle$ through bonds in the passive segment in a simulation. $\langle J \rangle$ is random in general, however, during the period when $\langle J \rangle$ is large, as shown in the inset, $\langle J \rangle$ exhibits successive peaks in accordance with the direction of the flux.

the motion of this segment as input to construct a time dependent protocol to modulate the configuration of an equivalent segment that is disconnected from the network and placed in a viscous fluid. We find that doing so creates a low Reynolds number ($Re$) swimmer. Using the diagrammatic theory introduced in Sec. V, we show that the swimming speed is in fact proportional to the energy flux. Using these results, we finally discuss the possibility that the energy conducting passive segment attached to our chiral active network, when immersed in a fluid, can act as a stalled swimmer and pump the fluid.

### A. Energy flux in a passive segment coupled to an active network

We expect that our chiral active network can still generate energy fluxes when some nodes along the transmission pathway are made *passive* (i.e. uncoupled from the active bath and magnetic field). Mimicking conventional paradigms to study heat conduction, which consider passive chain between two thermal baths with different temperatures (FIG. 4a), we connect a passive harmonic chain to our chiral active network (FIG. 4b). We indeed find that our chiral active network is able to generate a nonzero averaged energy flux through the passive material (FIG. 4c, Supplemental Video). From FIG. 4c and the Supplemental Video, the flux through the passive segment is in general stochastic. Although the direction of flux is from left to right on average, the instantaneous flux can also transport from right to left. During the period when $J$ is large, $J$ exhibits successive peaks, indicating a large CCW energy flow. The spacing between the peaks matches the sound speed of the passive chain.

### B. Nonreciprocal motion as a swimming protocol

The energy fluxes through the passive segment, especially the successive flux peaks observed in the above simulation, seem to suggest that stochastic wave like collective oscillations are responsible for the energy transfer. System with nonrecriprocal wave-like fluctuations when placed in contact with a viscous fluid, can act as low $Re$ swimmers [28–30]. Thus, the nonreciprocal motion in the passive segment could potentially be exploited as a strategy to enable locomotion. This idea is illustrated in FIG. 5a.

To pursue this idea, we consider a minimal passive elastic segment with three spheres arranged in a linear configuration [30]. We imagine instances where the passive elastic segment is disconnected from the chiral active network and immersed in a low-$Re$ fluid FIG. 5a. When the lengths of the two springs connecting the spheres, $L_1(t) = L + \Delta L_1(t), L_2(t) = L + \Delta L_2(t)$ are varied according to some prescribed protocol, the time-averaged swimming speed is (Eqn. (12) in [30])

$$V_s = \frac{7a}{24L^2} \left\langle \Delta L_1 \frac{\mathrm{d}\Delta L_2}{\mathrm{d}t} - \frac{\mathrm{d}\Delta L_1}{\mathrm{d}t} \Delta L_2 \right\rangle, \qquad (14)$$

where $a$ is the radius of the bead. Assumptions for this equation are $a/L \ll 1, \Delta L_i/L \ll 1$, and total external force on the swimmer is zero.

We now imagine recording the motions of the passive segment when it is connected to our chiral active network (FIG. 5a) and not coupled to a viscous fluid. This recorded motion can be used a protocol for modulating the configuration of an equivalent *swimmer* passive segment that is placed in a viscous fluid. We compute the swimming speed $V_s$ of the swimmer using Eqn. 14 and find that it is in fact proportional to the energy flux, $\langle J \rangle$, conducted through the passive segment when it is coupled to the chiral active network (FIG. 5b). The nonreciprocal motions that is responsible for energy fluxes can also be used as a protocol to generate motion in a low $Re$ fluid. The proportionality constant between the swim speed, $V_s$ and the energy flux, $\langle J \rangle$, can be calculated using a modified path analysis technique (Supplementary Material),

$$\frac{V_s}{7a/24L^2} = -\frac{k_0}{k} \frac{\langle J \rangle}{k/2}, \qquad (15)$$

where $k_0 = k_g + m/\tau^2$ ($B, \gamma = 0$ for the passive segment). This result Eqn. (15) holds beyond small-$k$ regime because all orders of paths are considered (Supplementary Material). FIG. 5b and Eqn. (15) together establish that

one can dictate swimmer's speed from the energy flux of active networks. Similar proportionality between $V_s$ and $J$ can be expected for other types of three-sphere swimmers, such as one where one sphere is much larger than the other two [31]. This is because the swim speed $V_s$ is generically proportional to the area enclosed in the $\Delta L_i$ space [32]. This area is also proportional to the energy flux $J$ (Supplemental Material).

### C. Coupling energy flux to fluid pumping

Finally, we now consider the scenario where the passive segment is immersed in a fluid (FIG. 5c). Since the segment is tethered by $k_g$ and is connected to the tethered active part, it cannot swim indefinitely. However, a tethered, stalled swimmers can potentially pump the fluid [33]. We would like to see whether our passive segment can, at least in theory, similarly act as a stalled swimmer and pump the fluid. Specifically, we consider how the tethering force and the coupling to the fluid affects the dynamics of the segment.

In the presence of tethering forces, Eqn. (14) for $V_s$ needs to be modified. Ref. [30] discussed swimmer with a constant external force $F$, and its Eqn. (39) says the modified swimming speed $V_s(F) = V_s + F/(6\pi\eta_f a)$, where $\eta_f$ is fluid's dynamic viscosity. Since this result is obtained under linearized hydrodynamics, it also applies to our stochastic case granted that we replace $F$ by its averaged value $\langle F\rangle$. This tells that we can first consider the untethered case, then adapt to the tethered case using the above formula.

In the presence of an added fluid, we desire that the original dynamics is not altered too much, otherwise both the energy flux and the correlation in Eqn. (15) would be distorted, and the $V_s \propto -\langle J\rangle$ result cannot be utilized. So we need a regime where the fluid, in spite of having a low $Re$, is perturbative. To make the fluid perturbative, we require the dissipation rate due to the viscous force to be much smaller than the energy flux through the segment. This can be expressed as $\eta_f a v^2 \ll J$, where $v$ is the characteristic velocity of the bead, $J$ is the energy flux in the absence of the fluid. To satisfy low $Re$ condition, one needs $Re = \rho_f a v/\eta_f \ll 1$, where $\rho_f$ is fluid's density. Writing these two conditions together, one gets $J \gg \eta_f a v^2 \gg \rho_f a^2 v^3$. This condition ignored hydrodynamic interactions between the beads, because it is a higher-order perturbation with the order of $a/L$. As a numerical example, this condition can be satisfied by setting $k = 5\times10^{-5} kg/s^2, k_g = 1\times10^{-6} kg/s^2$ for springs (value of optical trap), $a = 10^{-6}m$ for all beads (size used in [33]), $T_a = 10^{-18}J, \tau = 1s$ for the active bath [34], $\rho_f = 10^3 kg/m^3, \eta_f = 10^{-3} kg/(m\cdot s)$ for liquid (water), and $B = 10^{-5} kg/s$ for the $B$-field. From numerical calculations, $v = 3.8\times10^{-6} m/s$, and the three scales are $J = 5\times10^{-19} J/s, \eta_f a v^2 = 1.4\times10^{-22} J/s, a^2 v^3 \rho_f = 5.4\times10^{-29} J/s$, which does exhibit scale separations. If the separation between beads is $L = 10^{-7}m$, calculated pumping speed is $1\times10^{-8} m/s$. This speed can be scaled up by increasing $T_a$. The only suspicious parameter is $B$, which seems too strong in order to make $J$ sizable. To make practical use of this model, one should consider Lorentz force substitutes, such as gyroscopic force [14] or Coriolis force [35].

These discussions together suggest that, if the passive part is immersed in a perturbative fluid, it can generate fluid flows. Assuming the relaxation timescale of the active network is much faster than the timescale of swimming due to the small $V_s(F)$, one can expect the following process. Initially the passive part experiences $\langle F\rangle = 0$, so it swims with an average speed $V_s$; as the part drifts, $\langle F\rangle$ increases and acts in the direction of $-V_s$; when $\langle F\rangle \approx -6\pi\eta_f a V_s$, the swimmer is stalled. The stalled swimmer pumps fluid in direction $-V_s \propto \langle J\rangle$.

## VII. CONCLUSION

[Will be rewritten/revised after we converge on everything else]We have established that, our active gyroscopic network can rectify energy and control its rectification through network geometries. At last, we discuss possibilities to extend this model and provide outlooks.

In our theoretical treatment, the parameters are assumed uniform for all particles and bonds, which is not necessary. We only need $\tau, T_a$ to be uniform, and other parameters $m, k_g, k, B, \gamma$. can be nonuniform. If we add an additional white noise to the equation of motion Eqn. (1), the energy flux is not affected. As a comparison, in models that use OUP for directed particle transport, the additional white noise would usually suppress the rectification [36].

From Fourier mode analysis (Sec. IV), the ingredients for nonzero energy fluxes are nonreciprocal response and weighted excitation. The nonreciprocal response is introduced by Lorentz-like forces, and it makes theory tractable, since this force does not do work on the particles and is linear. The disadvantage is that its experimental realization is not easy. Inspired by these two ingredients, one can try other ways to achieve rectifications. One way is to replace the active particle with Lorentz force by active rotors. In this case the equation for energy flux Eqn. (7) would contain extra terms, and since rotors themselves are active, the active bath is not needed. Another possible way is to introduce nonlinearity, as nonlinearity can make nonreciprocal metamaterials (cite nonreciprocal). This has been exploited to make thermal diodes. One could imagine a setup that replaces the springs with these nonreciprocal materials, and add active bath but not Lorentz force to the connecting sites.

## ACKNOWLEDGEMENTS

We thank many people.

[1] Udo Seifert, "Stochastic thermodynamics, fluctuation theorems and molecular machines." Reports on progress in physics. Physical Society (Great Britain) **75**, 126001 (2012), arXiv:1205.4176v1.

[2] Ali Coskun, Michal Banaszak, R. Dean Astumian, J. Fraser Stoddart, and Bartosz A. Grzybowski, "Great expectations: Can artificial molecular machines deliver on their promise?" Chemical Society Reviews **41**, 19–30 (2011).

[3] C Jarzynski and O Mazonka, "Feynman's ratchet and pawl: An exactly solvable model." Physical review. E, Statistical physics, plasmas, fluids, and related interdisciplinary topics **59**, 6448–6459 (1999).

[4] A. Mogilner and G. Oster, "Cell motility driven by actin polymerization," Biophysical Journal **71**, 3030–3045 (1996).

[5] V. Y. Chernyak and N. A. Sinitsyn, "Pumping Restriction Theorem for Stochastic Networks," Physical Review Letters **101**, 160601 (2008).

[6] Saar Rahav, Jordan Horowitz, and Christopher Jarzynski, "Directed flow in nonadiabatic stochastic pumps," Physical Review Letters **101**, 1–4 (2008), arXiv:0808.0015.

[7] N. A. Sinitsyn and Ilya Nemenman, "Universal geometric theory of mesoscopic stochastic pumps and reversible ratchets," Physical Review Letters **99**, 1–4 (2007), arXiv:0705.2057.

[8] Yonatan Dubi and Massimiliano Di Ventra, "Colloquium: Heat flow and thermoelectricity in atomic and molecular junctions," Reviews of Modern Physics **83**, 131–155 (2011).

[9] C. Strohm, G. L. J. A. Rikken, and P. Wyder, "Phenomenological Evidence for the Phonon Hall Effect," Physical Review Letters **95**, 155901 (2005).

[10] Nianbei Li, Jie Ren, Lei Wang, Gang Zhang, Peter Hänggi, and Baowen Li, "Colloquium : Phononics: Manipulating heat flow with electronic analogs and beyond," Reviews of Modern Physics **84**, 1045–1066 (2012), arXiv:1108.6120.

[11] Kiyoshi Kanazawa, Takahiro Sagawa, and Hisao Hayakawa, "Heat conduction induced by non-Gaussian athermal fluctuations," Physical Review E **87**, 052124 (2013), arXiv:1209.2222v3.

[12] Welles A. M. Morgado and Sílvio M. Duarte Queirós, "Thermostatistics of small nonlinear systems: Poissonian athermal bath," Physical Review E **93**, 012121 (2016).

[13] Ignacio A. Martínez, Édgar Roldán, Luis Dinis, and Raúl Alberto Rica, "Colloidal heat engines: A review," Soft Matter **13**, 22–36 (2017).

[14] Lisa M. Nash, Dustin Kleckner, Alismari Read, Vincenzo Vitelli, Ari M. Turner, and William T. M. Irvine, "Topological mechanics of gyroscopic metamaterials," Proceedings of the National Academy of Sciences **112**, 14495–14500 (2015), arXiv:1504.03362.

[15] M. C. Marchetti, J. F. Joanny, S. Ramaswamy, T. B. Liverpool, J. Prost, Madan Rao, and R. Aditi Simha, "Hydrodynamics of soft active matter," Reviews of Modern Physics **85**, 1143–1189 (2013), arXiv:1207.2929.

[16] Anton Souslov, Benjamin C. van Zuiden, Denis Bartolo, and Vincenzo Vitelli, "Topological sound in active-liquid metamaterials," Nature Physics **13**, 1091–1094 (2017), arXiv:1610.06873.

[17] Suraj Shankar, Mark J. Bowick, and M. Cristina Marchetti, "Topological Sound and Flocking on Curved Surfaces," (2017), 10.1103/PhysRevX.7.031039, arXiv:1704.05424.

[18] Noah P. Mitchell, Lisa M. Nash, Daniel Hexner, Ari M. Turner, and William T. M. Irvine, "Amorphous topological insulators constructed from random point sets," Nature Physics (2018), 10.1038/s41567-017-0024-5.

[19] Étienne Fodor, Cesare Nardini, Michael E. Cates, Julien Tailleur, Paolo Visco, and Frédéric van Wijland, "How Far from Equilibrium Is Active Matter?" Physical Review Letters **117**, 038103 (2016), arXiv:1604.00953.

[20] Ching Hua Lee, Guangjie Li, Guliuxin Jin, Yuhan Liu, and Xiao Zhang, "Topological dynamics of gyroscopic and Floquet lattices from Newton's laws," Physical Review B **97**, 085110 (2018), arXiv:1701.03385.

[21] Peter Hanggi and Peter Jung, "Colored Noise in Dynamical Systems," in *Advances in Chemical Physics* (John Wiley & Sons, Ltd, 1994) pp. 239–326.

[22] Stefano Lepri, "Thermal conduction in classical low-dimensional lattices," Physics Reports **377**, 1–80 (2003).

[23] Ken Sekimoto, "Langevin Equation and Thermodynamics," Progress of Theoretical Physics Supplement **130**, 17–27 (1998).

[24] Crispin Gardiner, "The Ito Calculus and Stochastic Differential Equations," in *Stochastic Methods* (Springer-Verlag Berlin Heidelberg, 2009) 4th ed., Chap. 4, p. 107.

[25] Michele Ceriotti, Giovanni Bussi, and Michele Parrinello, "Colored-Noise Thermostats à la Carte," Journal of Chemical Theory and Computation **6**, 1170–1180 (2010).

[26] Anupam Kundu, Sanjib Sabhapandit, and Abhishek Dhar, "Large deviations of heat flow in harmonic chains," Journal of Statistical Mechanics: Theory and Experiment **2011** (2011), 10.1088/1742-5468/2011/03/P03007, arXiv:1101.3669.

[27] P. Pradhan and U. Seifert, "Nonexistence of classical diamagnetism and nonequilibrium fluctuation theorems for charged particles on a curved surface," EPL (Europhysics Letters) **89**, 37001 (2010), arXiv:0912.4697.

[28] G. Taylor, "Analysis of the Swimming of Microscopic Organisms," Proceedings of the Royal Society A: Mathematical, Physical and Engineering Sciences **209**, 447–461 (1951), arXiv:0912.1431.

[29] E. M. Purcell, "Life at low Reynolds number," American Journal of Physics **45**, 3–11 (1977), arXiv:1011.1669v3.

[30] Ramin Golestanian and Armand Ajdari, "Analytic results for the three-sphere swimmer at low Reynolds number," Physical Review E - Statistical, Nonlinear, and Soft Matter Physics **77**, 1–6 (2008), arXiv:0711.3700.

[31] R. Golestanian, "Three-sphere low-Reynolds-number swimmer with a cargo container," The European Physical Journal E **25**, 1–4 (2008).

[32] Ramin Golestanian and Armand Ajdari, "Stochastic low Reynolds number swimmers," Journal of Physics Condensed Matter **21** (2009), 10.1088/0953-8984/21/20/204104, arXiv:0901.1624.

[33] Marco Leoni, Jurij Kotar, Bruno Bassetti, Pietro Cicuta, and Marco Cosentino Lagomarsino, "A basic swimmer at low Reynolds number," Soft Matter **5**, 472–476 (2009),

arXiv:0807.1867.

[34] Xiao-Lun Wu and Albert Libchaber, "Particle Diffusion in a Quasi-Two-Dimensional Bacterial Bath," Physical Review Letters **84**, 3017–3020 (2000).

[35] H. Kählert, J. Carstensen, M. Bonitz, H. Löwen, F. Greiner, and A. Piel, "Magnetizing a Complex Plasma without a Magnetic Field," Physical Review Letters **109**, 155003 (2012).

[36] Roland Bartussek, Peter Reimann, and Peter Hänggi, "Precise numerics versus theory for correlation ratchets," Physical Review Letters **76**, 1166–1169 (1996).

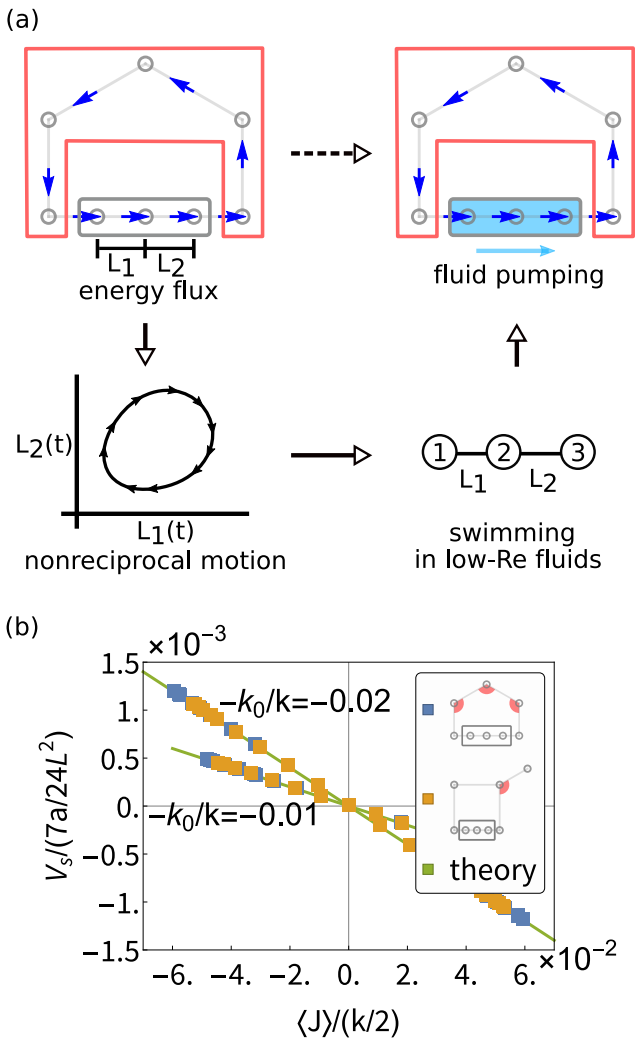


FIG. 5. Utilization of active network dynamics in low-Re swimming and fluid pumping (a) Flowchart of this section. We would like to utilize the energy flux to generate motions. To persue this goal, we start from the result that the active gyroscopic network can drive energy through a passive segment. The energy flux indicates nonreciprocal motions of the particles. Using this nonreciprocal motion as a swimming protocol, a low-Re swimmer can swim at a speed $V_s$. The nonreciprocal motion is a schematic for illustration purposes, and the real data is much more noisy. Finally by immersing the passive segment into a low Re fluid, it is possible to pump the fluid. (b) Swimmer's speed $V_s$ is proportional to the energy flux $\langle J\rangle$ in the active network. The proportionality constant is $-k_0/k$, which is independent of the network geometry. The series of dots for each $-k_0/k$ are obtained by varying the labelled angles (by red disk sectors) in pentagon networks or square+tail networks.